The Meteoritical Society

Meteoritics & Planetary Science 1–11 (2014)
doi: 10.1111/maps.12321

Infrared imaging spectroscopy with micron resolution of Sutter's Mill meteorite grains

Mehmet YESILTAS[1*], Yoko KEBUKAWA[2], Robert E. PEALE[1], Eric MATTSON[3], Carol J. HIRSCHMUGL[3], and Peter JENNISKENS[4,5]

[1]Department of Physics, University of Central Florida, Orlando, Florida 32816, USA
[2]Faculty of Engineering, Yokohama National University, 79-5 Tokiwadai, Hodogaya-ku, Yokohama 240-8501, Japan
[3]Department of Physics, University of Wisconsin-Milwaukee, Milwaukee, Wisconsin 53211, USA
[4]SETI Institute, Mountain View, California 94043, USA
[5]NASA Ames Research Center, Moffett Field, California 94035, USA
[*]Corresponding author. E-mail: myesiltas@knights.ucf.edu

(Received 04 February 2014; revision accepted 03 May 2014)

Abstract–Synchrotron-based Fourier transform infrared spectroscopy and Raman spectroscopy are applied with submicrometer spatial resolution to multiple grains of Sutter's Mill meteorite, a regolith breccia with CM1 and CM2 lithologies. The Raman and infrared active functional groups reveal the nature and distribution of organic and mineral components and confirm that SM12 reached higher metamorphism temperatures than SM2. The spatial distributions of carbonates and organic matter are negatively correlated. The spatial distributions of aliphatic organic matter and OH relative to the distributions of silicates in SM2 differ from those in SM12, supporting a hypothesis that the parent body of Sutter's Mill is a combination of multiple bodies with different origins. The high aliphatic CH_2/CH_3 ratios determined from band intensities for SM2 and SM12 grains are similar to those of IDPs and less altered carbonaceous chondrites, and they are significantly higher than those in other CM chondrites and diffuse ISM objects.

INTRODUCTION

The Sutter's Mill (SM) meteorite is a regolith breccia composed of a variety of CM1 and CM2 clasts in a CM type matrix (Jenniskens et al. 2012; Zolensky et al. 2014). The meteorite is officially classified as a "C" chondrite. The material is of interest because it represents surface material from a primitive asteroid, the target of upcoming space missions OSIRIS-REx and Hayabusa 2. The fall occurred in El Dorado County in California on 22 April 2012, and the first three meteorites were found before rains hit the area (now numbered SM1, 2, and 3). In total, 77 meteorites were recovered from this fall. Meteorite SM12 was collected from the field during a volunteer search coordinated by NASA Ames Research Center.

An initial study by members of the Sutter's Mill meteorite consortium found that individually recovered meteorites showed a range for the signatures of aqueous alteration and thermal metamorphism (Jenniskens et al. 2012). Based on Raman spectra of macromolecular carbon and using the method of Cody et al. (2008), Marc Fries and coworkers found that parts of SM2 experienced temperatures no higher than 153 ± 27 °C, whereas SM12 reached up to 268 ± 42 °C. As part of this study, Monica Grady and coworkers found that SM contains the lowest known $\delta^{15}N$ (ratio of stable isotopes $^{15}N/^{14}N$) among CM2 chondrites, which may mean that SM has N-bearing organic molecules whose compositions are different than those in other CM2 chondrites.

These temperature history and compositional differences immediately raise questions about how they occurred and what they may tell us about the formation and evolution of the CM chondrite parent body. For example, individual clasts may sample different

temperature and aqueous alteration histories on the surface of the parent body. Another possibility is that the Sutter's Mill meteorite is an aggregate of fragments that originated from different parent body asteroids, or perhaps even of comets (Jenniskens et al. 2012).

In this paper, we investigate the thermal and aqueous alteration history of SM materials further using synchrotron-based Fourier transform infrared (FTIR) microspectroscopy in the range of 3850–900 cm^{-1} and micro-Raman spectroscopy in the range of 2200–800 cm^{-1}. Spectral signatures and spatial distribution of organics and minerals are investigated in situ in multiple grains from SM2 and SM12, mapping the different functional groups with submicron spatial resolution. This work compliments the infrared studies by Sandford et al. (2013) and Nuevo et al. (2014), which investigated differences among SM meteorites on a larger spatial scale.

SAMPLES AND EXPERIMENTAL DETAILS

We received samples of SM2 and SM12 in the form of chips through the Sutter's Mill meteorite consortium. SM2 was found by one of us (PJ) in fragmented form on the surface of a parking lot, likely crushed by a car (Jenniskens et al. 2012). It was collected in aluminum foil and stored in a freezer at NASA Ames prior to rain hitting the area, but it may have been contaminated to some extend by the asphalt of the parking lot surface and any other organic material that came in contact with the meteorite, such as a car tire and compounds in the air. Nevertheless, Zolensky et al. (2014) reported finding oldhamite in a small chip of SM2, a mineral very sensitive to water. Our sample of SM2 came from an internal part of the rock, which had no direct contact with the asphalt surface. Studies of amino acids (Burton et al. 2014), which are present in the meteorite at only very low level, showed that SM2 and SM12 may contain amino acids of terrestrial origin, but the extent of the contamination is ambiguous.

The fully crusted SM12 was recovered after the heavy rain (Jenniskens et al. 2012). It was found stuck on a narrow side path in (dried up) muddy soil, from which the porous meteorite may have picked up contaminants. It was briefly touched, then collected in aluminum foil and stored in a freezer at NASA Ames Research Center. The SM12 chip studied here came from the center of a stone, at least 0.5 cm from the nearest fusion crust.

We ground each sample in a mortar and pestle down to tens of micrometer size grains. These grains are expected to represent the different lithologies in the chips studied here. Subsequently, these grains were placed on a diamond window, which was placed under the infrared microscope for transmission measurements, or on a silicon substrate for micro-Raman measurements.

Micro-Raman spectra of Sutter's Mill samples were collected in situ at the Materials Characterization Facility at University of Central Florida using a Renishaw spectrometer coupled to a Leica DMLM microscope using Ar ion laser excitation at 514.5 nm wavelength. Total laser power of 20 mW was focused to a 4 μm^2 spot, so that the intensity on the sample was 5 $mW/\mu m^2$. A 5× objective was used to locate a meteorite grain of interest, and then a 50× objective was used to collect the spectrum. The spectrometer was calibrated using a silicon substrate with a Raman band at 521 cm^{-1}. All grains were measured three times between 2200–800 cm^{-1} with an integration time of 30 s.

The FTIR microspectroscopy was performed at the Synchrotron Radiation Center (SRC) in Stoughton, WI, using the IRENI beamline (Nasse et al. 2007, 2011). The beamline collects a large fan of bending magnet radiation to homogeneously illuminate a commercial focal plane array (FPA) detector. A Bruker Hyperion 3000 IR microscope was used in conjunction with a Bruker Vertex 70 FTIR spectrometer. Transmission measurements were performed using a 74× magnification objective with numerical aperture (NA) of 0.65. This optical arrangement corresponds to an effective geometric pixel size of 0.54 μm, so that the spatial resolution is diffraction-limited over the entire mid-IR region. Spectra were recorded with 4 cm^{-1} resolution using 128 coadded scans. A clean, sample-free region of the diamond window was used for reference spectra.

RESULTS

Raman Spectroscopy

The structural order of the carbonaceous material in each grain was inferred from the Raman peak positions, intensities, and widths of D (disordered) and G (graphite) bands, which are located near 1370 and 1600 cm^{-1}, respectively (Busemann et al. 2007). The D band is due to disordered sp^3 carbons, whereas the G band is due to graphite-like sp^2 carbon bonds (Suzuki et al. 2010). The spectra of 5 grains from each SM fragment in the region of 2200–800 cm^{-1} are presented in Fig. 1. Spectra are offset vertically from each other for clarity. Vertical lines indicate the positions of the D and G bands. A linear baseline was subtracted from each spectrum, which was then fit to a pair of Lorentzians to determine peak characteristics such as peak centers, widths, and relative intensities of the D and G bands.

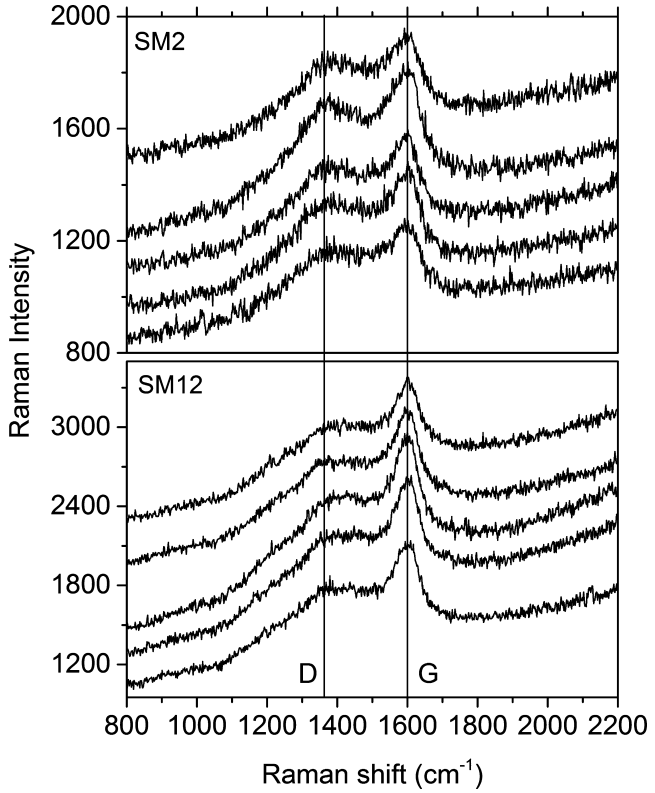

Fig. 1. Micro-Raman spectra of multiple SM2 and SM12 grains from the Sutter's Mill meteorite.

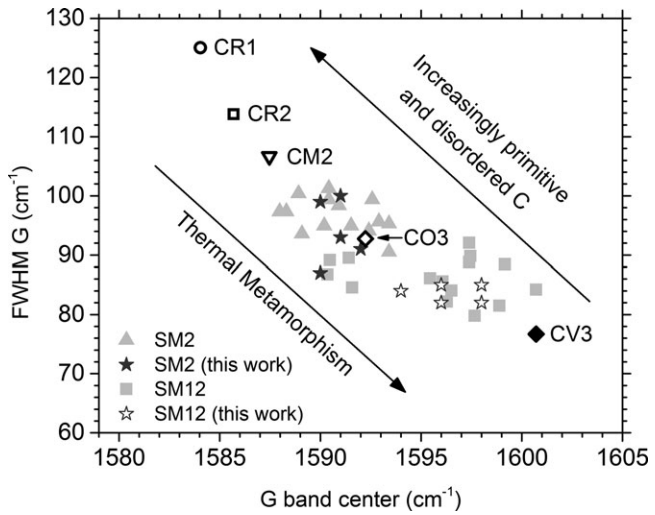

Fig. 2. FWHM of G-band versus the G-band center for SM2 and SM12 grains from this study plotted with data by Marc Fries (from Jenniskens et al. 2012).

Figure 2 presents the full width at half maximum (FWHM) of the G band versus its center frequency. Our results for SM2 and SM12 grains are in good agreement with data from Fries and coworkers presented in Jenniskens et al. (2012). The trends marked by arrows characterize the degree of thermal metamorphism and disorder of the carbon (Busemann et al. 2007; Jenniskens et al. 2012). According to Fig. 2, the G bands of SM2 grains are all wider and redder than those of the SM12 grains studied here. Increasing disorder of C is known to red shift the G band (Busemann et al. 2007). Thus, we confirm from different parts of the meteorites SM2 and SM12 than studied by Fries et al. (2014) that the macromolecular carbon in SM2 is relatively more disordered and SM12 is thermally more metamorphosed. SM2 and SM12 show evidence of heating to an intermediate degree while CR1, CR2, and CM2 chondrites show relatively less thermal alteration, unlike CV3 chondrites (Fig. 2).

Cody et al. (2008) proposed a thermometry that combines Raman spectroscopy with thermometric relationship by Busemann et al. (2007), and they obtained the following relationship between effective metamorphism temperature (T_{EFF}) and Raman G-band FWHM (Γ_G),

$$T_{EFF}(^{\circ}C) = 1594.4 - 20.4\Gamma_G + 5.8 \times 10^{-2}\Gamma_G^2. \quad (1)$$

Raman G-band FWHM of our SM2 grains varies from 87 to 100 cm^{-1}, and from 82 to 85 cm^{-1} for SM12 grains. Using these parameters and Equation (1), we obtained T_{EFF} = 134–259 °C for SM2 grains, and T_{EFF} = 279–312 °C for SM12 grains. These values are in good agreement with the values of 153 ± 27 °C for SM2 and 268 ± 42 °C for SM12 reported earlier (Jenniskens et al. 2012).

Infrared Spectroscopy

The spatially resolved infrared spectra of SM2 and SM12 grains show variations due to the compositional heterogeneity. Figure 3 presents representative infrared spectra of different SM2 and SM12 grains, each approximately 15–30 μm in diameter. Labels enumerate the individual grains that appear in our field of view. Our assignments of the observed IR absorption bands, following Salisbury et al. (1991), are summarized in Table 1. The strongest feature in all spectra (except SM12 grain #1) is a broad band centered around 1080–900 cm^{-1} due to Si-O stretching vibrations within silicate minerals. Most spectra also exhibit a broad band centered around 1500–1400 cm^{-1} due to asymmetric stretching vibrations of the CO_3^{2-} ion within carbonate minerals, a band at 1640 cm^{-1} due to the H-O-H bending modes of water, and a broad band around 3700–3000 cm^{-1} due to O-H stretching modes. Some spectra reveal weak but sharp structures in the range 3000–2800 cm^{-1} due to the C-H stretching

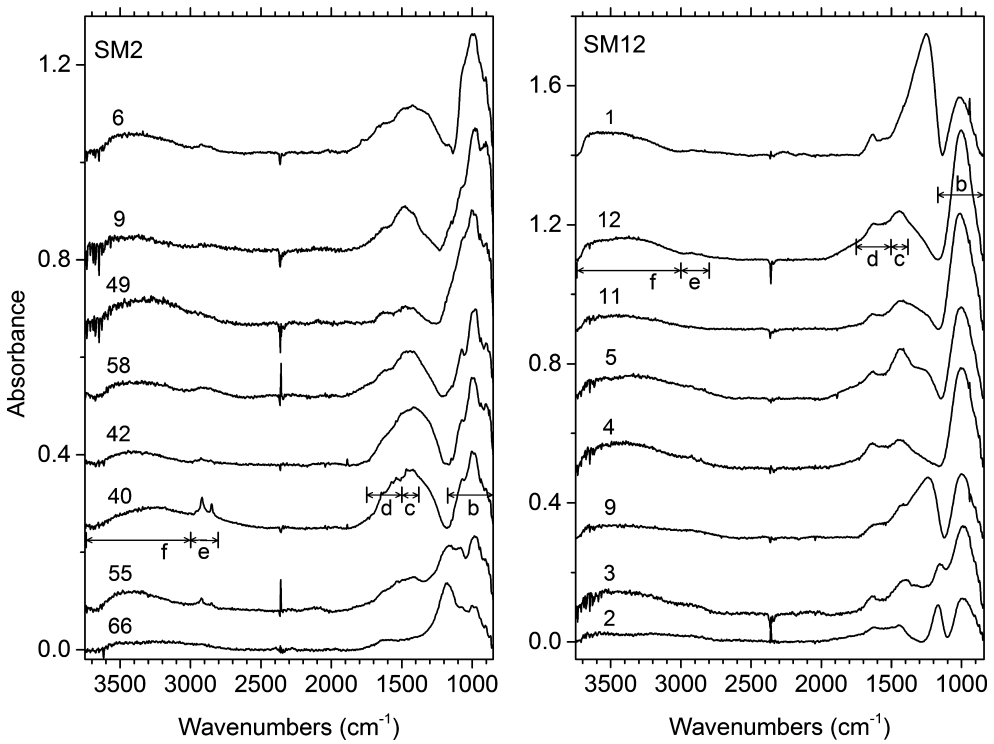

Fig. 3. IR absorbance spectra of individual SM2 and SM12 grains. Each spectrum is offset vertically for clarity. Numeric labels enumerate the grains in the field of view. Lettered horizontal bars indicate integration ranges for the corresponding spatial distribution maps in Figs. 4 and 5 for the two grains so analyzed.

Table 1. Positions and interpretation of the observed infrared bands.

Position (cm^{-1})	Mode	Assignment
870–910	Si-O	Olivine
950–1000	Si-O	Olivine + pyroxene + phyllosilicates
1070–1080	Si-O	Pyroxene
1150–1180	SO_4	Sulfates?
1240	Unknown	Unassigned
1410–1480	CO_3	Carbonates
1625	C=C	Aromatic hydrocarbon
1640–1650	H-O-H	Water
2350	CO_2	Atmospheric artifact
2800–3000	C-H	Aliphatic hydrocarbon
3000–3700	O-H	Water
3650	O-H	Phyllosilicates

vibrational modes within aliphatic hydrocarbons. Most of the bands tend to be broad in these spectra because each such band represents the average over the grain of different minerals from the same group (e.g., different carbonates).

In Fig. 3, there are three main peaks observed within the Si-O stretching region of SM2. These appear at 1080–1070 cm^{-1}, 1000–970 cm^{-1}, and 900 cm^{-1}, which are assigned to pyroxene, pyroxene + olivine, and olivine, respectively. Unlike SM2, infrared spectra of SM12 grains present a single band at approximately 1000 cm^{-1}, and a small structure appears near 3650 cm^{-1} due to O-H. These are typical features of phyllosilicates. The presence of a phyllosilicate O-H feature at 3650 cm^{-1} in spectra of SM2 grains is more ambiguous, suggesting lesser phyllosilicate abundances.

Shape and position of the carbonate band varies with carbonate species. For instance, the band center in dolomite appears at higher frequencies than in calcite. Absorbance bands in the spectra of SM2 and SM12 grains near 1450 cm^{-1} suggest an abundance of carbonates. Compared to the spectra of SM12 grains, SM2 grains have broader absorbance bands with more spectral variations near the carbonate region, which indicates a greater variety of carbonate species in SM2 grains than in SM12.

All Sutter's Mill meteorite grain spectra show absorbance bands between 3700-3000 cm^{-1} and at 1640 cm^{-1} due to H-O-H stretching and bending vibrational modes of water, respectively. A weak feature at 3650 cm^{-1} is observed in spectra of SM12 grains due to structural O-H in phyllosilicates, as already noted. We remark that the contribution of telluric water absorbed by minerals in SM12 meteorite should be very

low, because the absorbed water evaporates very quickly from the small grains. The band at 1640 cm^{-1} likely also includes significant contributions from carbonyl (C=O) and aromatics (C=C), which appear near 1700 cm^{-1} and 1600 cm^{-1}, respectively. The carbonyl band near 1700 cm^{-1} (Kebukawa et al. 2010) amounts to only a small bump or shoulder in some spectra, so that its comparatively insignificant contribution will be ignored in the subsequent discussion. Spectra of a few SM2 grains show aliphatic C-H stretching peaks between 3000 and 2800 cm^{-1} due to organics, but these peaks are very weak in spectra of SM12 grains.

Some spectra in both SM2 and SM12 show a band centered at 1180–1150 cm^{-1}. The origin of this band is currently unknown, but it is within the range of sulfates (Salisbury et al. 1991). Some SM12 spectra show a large band at 1240 cm^{-1}, which is also currently unidentified.

Spatial Distributions

Absorbance maps of specific infrared absorption bands reveal the spatial distributions and relationships between different minerals and organic molecules within individual meteorite grains (e.g., Yesiltas et al. 2013). We present such maps for one grain from each of SM2 and SM12, whose grain-averaged spectra were presented in Fig. 3. We integrated the spectrum for each individual pixel over ranges given in Table 2 and indicated in Fig. 3 (for the two grains studied) by horizontal lettered bars. Infrared absorbance maps of specific functional groups for SM2 grain #40 and SM12 grain #12 are presented in Figs. 4 and 5, respectively.

For instance, for carbonates we integrated from 1500 to 1380 cm^{-1}. In these spectra of individual pixels, the carbonate bands can be narrower than the full 120 cm^{-1} width of the integration window. However, this window ensures that we catch the carbonate band, wherever its center frequency happens to be. This allows the automatic analysis of thousands of spectra, without having to separately inspect each one, with good confidence that the result represents carbonate intensity.

Figure 4a presents the visible microscope image of SM2 grain #40. The other parts of Fig. 4 are infrared images giving spatial distributions for different compounds in this grain. The negative correlation between carbonates (Fig. 4c) and H_2O + aromatic C=C (Fig. 4d) is very strong. The negative correlation between carbonates and CH (Fig. 4e) is also strong. There is no significant correlation between H_2O + aromatic C=C stretch (Fig. 4d) and OH (Fig. 4f), which should be due to both water and phyllosilicates. This confirms the significant contribution from aromatic C=C, besides the H_2O, in the 1750–1500 cm^{-1} integration range. There exists a somewhat positive correlation between aliphatic C-H (Fig. 4e) and silicates (Fig. 4b). There is no significant correlation between aliphatic C-H and OH (Fig. 4f).

Table 2. Integration ranges for spatial distribution maps.

Group	Integration range (cm^{-1})
OH	3750–3000
Aliphatic CH	3000–2800
H_2O + aromatics	1750–1500
Carbonates	1500–1380
Silicates	1170–850

Figure 5a presents a visible microscope image of SM12 grain #12 together with infrared images giving spatial distributions of different compounds in SM12 grain #12. Here, too, the carbonates (Fig. 5c) and H_2O + aromatic C=C (Fig. 5d) have a very strong negative correlation, and the negative correlation between carbonates and aliphatic CH (Fig. 5e) is also strong. In contrast with SM2, here H_2O + aromatic C=C (Fig. 5d) are negatively correlated with OH (Fig. 5f). Unlike SM2 grains, SM12 grains present a weak infrared band near 3650 cm^{-1} due to phyllosilicates, but its contribution to the integrated absorbance is minor.

CH_2/CH_3 Ratios

The C-H stretching vibrational modes of aliphatic hydrocarbons are responsible for the weak but comparatively sharp infrared absorbance bands between 3000 and 2800 cm^{-1}. There are four peaks in this region, two for CH_2 (at 2854 and 2917 cm^{-1}) and two for CH_3 (at 2870 and 2952 cm^{-1}). After subtracting a linear baseline in the 3000–2800 cm^{-1} region, we obtained the CH_2/CH_3 ratios from the peak heights for SM2 (grain #40) and SM12 (grain #12) to be 4.00 ± 0.06 and 2.44 ± 0.07, respectively.

DISCUSSION

Thermal and Aqueous Metamorphism

SM2 shows IR signatures of pyroxene, olivine, and carbonates. In contrast, SM12 shows mainly carbonates and phyllosilicates with hardly any evidence for pyroxene and olivine. These observations are in agreement with Sandford et al. (2013) and Nuevo et al. (2014). Typical CM2 chondrites lack significant carbonate, pyroxene, or olivine IR signatures. Instead, they are dominated by phyllosilicates (Sandford 1984; Osawa et al. 2005; Beck et al. 2010). Only the unusual CM2 chondrite Bells and the ungrouped C-chondrite

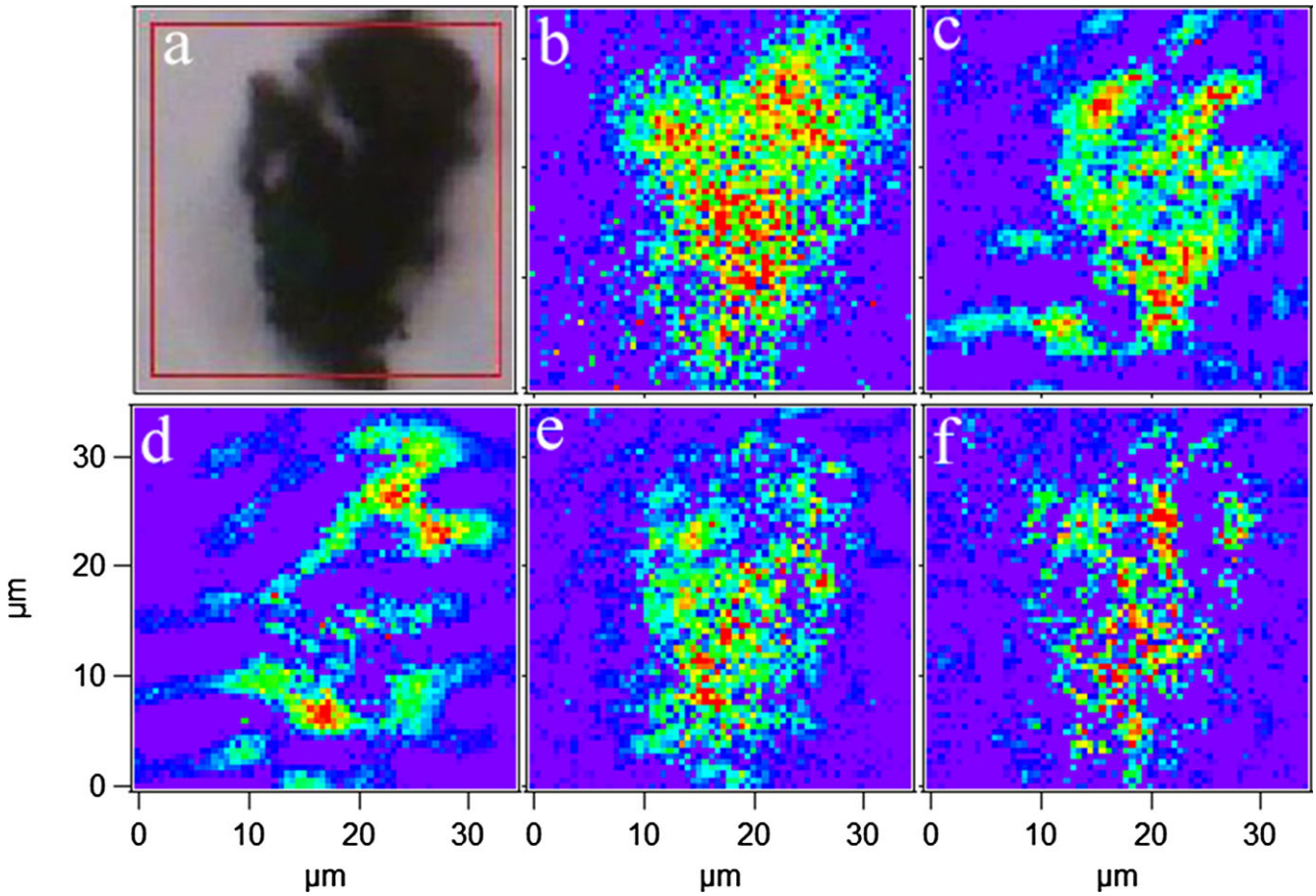

Fig. 4. Spatial distributions of characteristic absorbance in SM2 grain #40: a) visible micrograph; b) silicates, c) carbonates, d) H_2O + aromatic C=C stretch, e) aliphatic C-H stretch, f) OH.

Tagish Lake have significant infrared carbonate and phyllosilicate features simultaneously (Matrajt et al. 2004; Kebukawa et al. 2009a, 2010). On the basis of carbonates, SM2 and SM12 are more like Bells and Tagish Lake than they are like typical CM2s. However, on the basis of phyllosilicates, SM2 is not like Bells or Tagish Lake.

The Raman spectra reveal that organic matter in SM2 is more primitive and less thermally metamorphosed than in SM12 (Fig. 2). The mean G-band FWHM for SM2 grains falls close to the value for CO3 chondrites, while the mean G-band FWHM for SM12 grains falls between the values for CO3 and CV3. As pointed out before, these results imply that the Sutter's Mill meteorite was heated more than typical CMs (Jenniskens et al. 2012).

Some CM chondrites have been heated more than others, e.g., the so-called "heated-CM chondrites," whose aqueous alteration was followed by heating above 500 °C (Akai 1992). These exhibit evidence of secondary olivine produced by dehydration of phyllosilicates (e.g., Nakamura 2005). SM2 is less thermally metamorphosed than SM12, according to the analysis of our Raman spectra. Yet SM2 is dominated by the anhydrous silicates olivine and pyroxene while SM12 is dominated by phyllosilicates. Hence, the anhydrous silicates in SM2 are unlikely due to simple heating of material that was originally like SM12. This suggests different mineralogical history and precursor material for SM2 and SM12. In fact, Zolensky et al. (2014) suggested physical mixing of C and E type asteroids based on the abundance of oldhamite, phosphides, and enstatite in Sutter's Mill. Our observations provide additional evidence and support the possibility that SM2 and SM12 are not both CM chondrites.

Olivine in SM2 grains might be the dehydration product of phyllosilicates. However, secondary olivine cannot be formed at the temperature lower than approximately 500 °C (Nakamura 2005). On the other hand, even such heating events as experienced by some of the heated CMs does not change Raman G-band

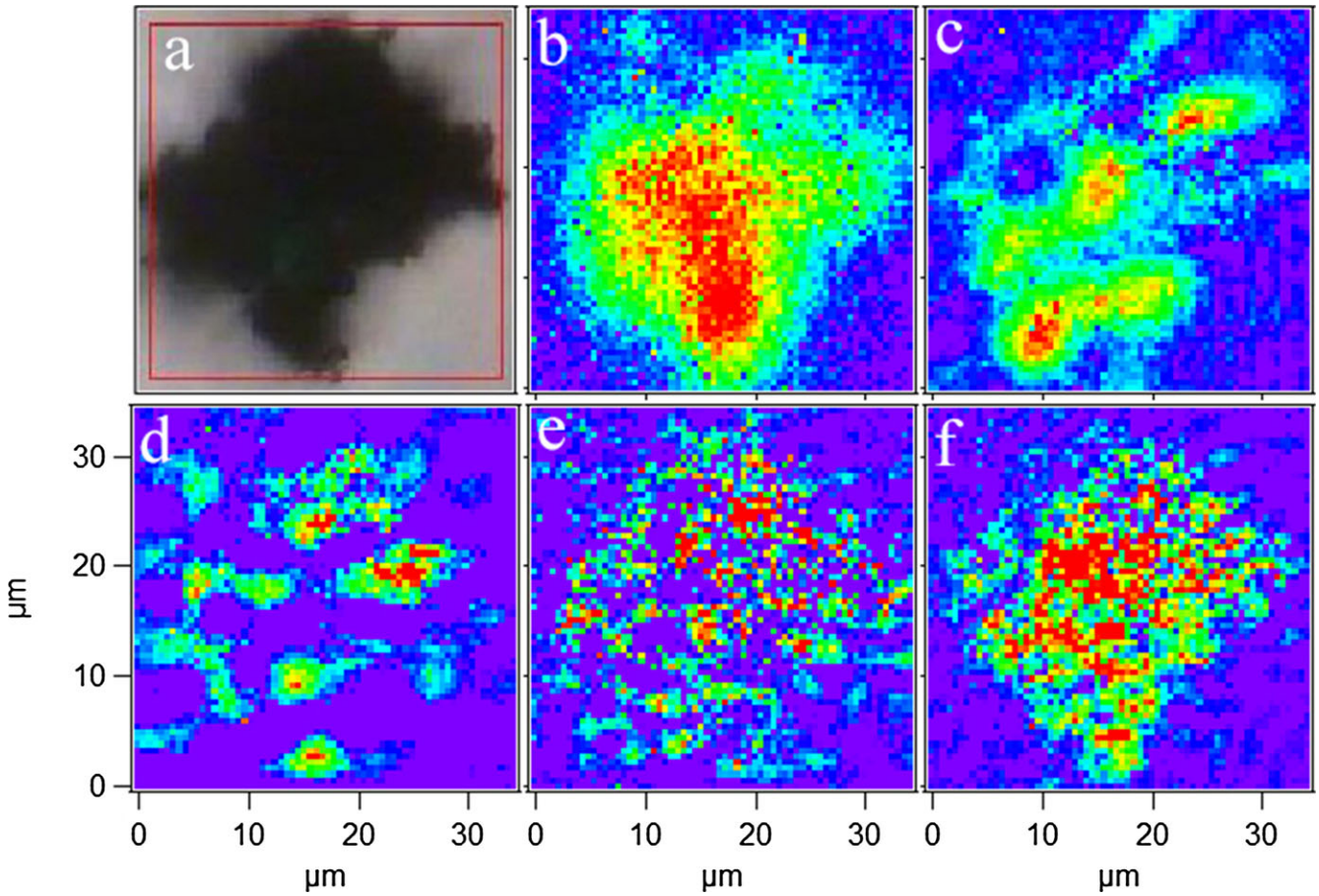

Fig. 5. Spatial distributions of characteristic absorbance in SM12 grain #12: a) visible micrograph; b) silicates, c) carbonates, d) H_2O + aromatic C=C stretch, e) aliphatic C-H stretch, f) OH.

characteristics significantly from those of nonheated CMs, in comparison to the thermally metamorphosed COs and CVs. For example, the G-band FWHM of Yamato 86720 (a CM heated over 750 °C) is 96.0 ± 0.2 cm^{-1}, which falls within the range of values for nonheated CMs (Busemann et al. 2007). Therefore, the T_{EFF} of 134–259 °C obtained from G-band FWHM of SM2 grains might be underestimated. This possibility is due to the assumption for the T_{EFF} calculation that isothermal heating of a parent body occurred for approximately 10^7 years, which may not be the case in the Sutter's Mill meteorite parent body or bodies.

Raman spectra show that heating in SM was more severe than for CMs but less severe than for most of the heated CMs. Heating events in the latter are considered to be short-duration events (Nakato et al. 2008), as might be due to impacts. Heating of regular CMs is considered to be long term at much lower temperatures (Huss et al. 2006). It is reasonable to suppose that the duration and temperature of heating for SM was intermediate between usual CMs and heated CMs.

Sutter's Mill entered Earth's atmosphere at high speed (28.6 km/s) and broke at a high altitude (Jenniskens et al. 2012). Based on the uneven fusion crust on most of the SM meteorites, they continued to fragment on the way down. Thermoluminescense (TL) measurements by Derek Sears and coworkers (consortium study, Jenniskens et al. 2012) showed that SM2 was heated to 300 ± 20 °C to a depth of 5–6 mm below the fusion crust, without the approximately 0.2 Ma needed for TL to recover. This heating could have been due to the entry, or because of solar heating near perihelion in the past <0.2 Ma (Jenniskens et al. 2012). In either case, it is unlikely that such heating could cause the degree of thermal metamorphoses inferred from the Raman spectra, since this would require more prolonged (>1 Ma) heating at these relatively low temperatures.

Some Sutter's Mill meteorites were exposed to heavy rain for several days. Generally, rain quickly oxidizes the iron content. Rain may also hydrate anhydrous minerals, but this takes significantly longer

and requires higher temperatures than was possible for those SM samples. Thus, SM12 hydrated silicate bands near approximately 1000 cm^{-1} (Fig. 3) cannot be attributed to hydration of anhydrous silicates by rain.

The OH stretching band for SM2 grains is systematically different than for SM12 grains. Specifically, the band center for SM2 grains appears near 3380 cm^{-1} while that for SM12 grains appears near 3450 cm^{-1}. This is in agreement with Takir et al. (2013) that the OH band in olivine- and pyroxene-rich meteorites appears at lower frequencies.

Differences in linewidths are also potentially interesting, since differences in inhomogeneous broadening may indicate differences in parent body processing history. Vibrational lines are broader in amorphous solids than in crystals of the same chemical composition. For grain-integrated spectra (Fig. 3) widths of characteristic bands tend to be broad, but there are clear differences between different grains. Bands in spectra from individual pixels tend to be sharper. To compare our bandwidths with those from independent measurements, we note that Flynn et al. (2013) presented infrared transmittance spectra with spot size of 7 μm × 7 μm for SM20 and SM30 meteorites. We converted their spectra to absorbance so that quantitative full width at half maxima could be obtained independent of absorption strength. Next, we obtained from our data a number of infrared spectra for different 7 μm x 7 μm areas of one SM12 grain for comparison. The results for five spectra in Flynn et al. (2013) and for five of ours show full width at half maxima for the carbonate band of 91 ± 18 and 99 ± 11, respectively. These widths are the same within the statistical uncertainty.

Spatial Relationships

Our investigation of spatial relationships between different compounds is preliminary and qualitative, since just two grains were analyzed. Future work will perform quantitative numerical correlation analysis on the approximately 20 grains for which we have already collected a large amount of data for both meteorites. Nevertheless, the preliminary results presented here allow a few notable observations and demonstrate the potential of the technique. A sense of the correlations is most easily obtained by viewing rapidly alternating pairs of images, while watching the blinking of concentration hot spots. The most prominent observation is the strong negative correlation between carbonates and H_2O + aromatic C=C for both grains. Similarly, the spatial correlation of carbonates and aliphatic C-H is negative.

Association of aliphatic organic matter with phyllosilicates is shown in Bells (Kebukawa et al. 2009a, 2010); in NWA 852 (Yesiltas et al. 2013); in CI1, CM2 chondrites; as well as Tagish Lake (Pearson et al. 2002, 2007). We observed in SM2 grain #40 that the spatial distribution of aliphatic C-H only partially overlaps with that of silicates, while the overlap between aliphatic CH and OH is even less. Thus, aliphatic organic matter is not strongly correlated with phyllosilicates in SM2 grain #40, in contrast to Bells, NWA 852, and Tagish Lake.

In SM12 grain #12 the overlap between silicates and aliphatic CH is even less than in SM2 grain #40. If significant, it suggests that the aqueous alteration history for SM12 differs from that of SM2, supporting the hypothesis that the parent body of the Sutter's Mill meteorite is a combination of multiple parent bodies.

Spatial distributions of silicates and OH in SM2 grain #40 only partially overlap, which is probably due to the abundance of anhydrous silicates indicated by the infrared spectrum (Fig. 3). In contrast, for SM12 grain #12 the correlation between silicates and OH seems somewhat stronger, consistent with the abundant phyllosilicates indicated by the infrared spectrum (Fig. 3).

C-H Stretching Band Ratios

Peak intensity ratio of asymmetric CH_2 to CH_3 bands can be used to roughly infer aliphatic chain lengths and/or branching levels (Igisu et al. 2009), which are affected by processing. For instance, energetic particles may break bonds, and heating may aromatize aliphatic molecules, both of which shorten chain lengths and give lower CH_2/CH_3 ratios (Merouane et al. 2012). Fewer aromatics and higher CH_2/CH_3 ratios suggest dense clouds and/or protosolar nebular processes (Sandford et al. 2006). The higher ratio for SM2 than for SM12 suggests that the aliphatic organics in these materials may have different origins and/or have undergone different parent body processing. Our results suggest that SM12 was subjected to higher metamorphism temperatures (T_{EFF} = 279–312 °C) than SM2 (T_{EFF} = 134–259 °C), which is consistent with the lower CH_2/CH_3 ratio for SM12.

The aliphatic type organic matter in Sutter's Mill is largely different from that in CM and CI chondrites. The CH_2/CH_3 ratios of various astronomical objects were previously reported (Table 3). The measured ratio is close to 1.0 for CM chondrites, but around 2.5 for cometary dust and interplanetary dust particles. The high ratios for SM2 and SM12 are closer to those of interplanetary dust and cometary matter, as well as to some other carbonaceous chondrites. The ratio for Tagish Lake (3.0) is in between that of SM2 and SM12. We note that the CH_2/CH_3 ratio of Tagish Lake IOM

Table 3. The CH_2/CH_3 ratios of SM meteorites and various astronomical objects.

Objects	CH_2/CH_3 band strength ratio	Source
SM2 (grain #40)	4.00 ± 0.06	This work
SM12 (grain #12)	2.44 ± 0.07	This work
Comet Wild 2 coma dust	2.5 ± 0.1	Keller et al. (2006)
Anhydrous IDPs	2.46 ± 0.01	Flynn et al. (2003)
Hydrated IDPs	2.31 ± 0.01	Flynn et al. (2003)
NWA 852 (CR2)	2.53 ± 0.05	Yesiltas et al. (2013)
Tagish Lake (C)	3.0[a]	Matrajt et al. (2004)
DISM	1.17 ± 0.2[b]	Sandford et al. (1991)
Paris (CM)	1.8 ± 0.2	Merouane et al. (2012)
Orgueil (CI)	1.4 ± 0.1	Kebukawa et al. (2010)
Bells (CM, anom.)	1.4 ± 0.2	Kebukawa et al. (2010)
Murchison (CM)	1.0 ± 0.1	Kebukawa et al. (2010)

[a]Recalculated.
[b]Average.

was recently re-evaluated after IOM extraction via solvents to be in the range 1.2–1.9 (Alexander et al. 2014). However, CH_2-rich material in the bulk Tagish Lake may be lost during the IOM purification processes, causing ratios determined using this procedure to be systematically underestimated in comparison to those determined by analysis of organics in situ.

The high CH_2/CH_3 ratios in SM2 and SM12 are consistent with reports that organic matter in Sutter's Mill is unique among typical CM and other primitive chondrites. First, laboratory hydrothermal treatment of Sutter's Mill caused release of complex polyether- and ester-containing alkyl molecules which were never before detected in meteorites (Pizzarello et al. 2013). Second, a bimodality in the C release suggests a combination of volatile-rich and volatile-poor organic components (Jenniskens et al. 2012). Third, C and N isotopic ratios vary widely between different SM fragments (Jenniskens et al. 2012).

The similarity to cometary organics is of particular interest, because the preatmospheric orbit of Sutter's Mill, like that of CM chondrite Maribo, was very similar to that of a Jupiter-family comet 2P/Encke, having a Tisserand parameter on the border of the comet and asteroid fields (Jenniskens et al. 2012). It has been argued that these meteorites may originate, in fact, from Jupiter-family comets (Haack et al. 2010).

A possible source of uncertainty regarding CH_2/CH_3 ratios is contamination, to which the spectral region of the C-H stretch is susceptible (Kebukawa et al. 2009b). This may be a particular issue for SM2, which was recovered from an asphalt surface. The C-H stretch absorption is in fact stronger for *some* of the SM2 grains than for any of the SM12 grains that we studied here. However, we remind that all grains studied in this paper were extracted from the interior of the meteorite, while it was the exterior that contacted the asphalt surface. Also, the amino acid analysis (Burton et al. 2014) suggests a higher contamination for SM12 than for SM2.

A second source of uncertainty in the ratios is that overtones of the strong absorption bands at lower frequencies overlap the aliphatic C-H stretching bands in the 2980–2870 cm^{-1} region (Nuevo et al. 2014). However, the low-frequency bands, which include contributions from many different chemical moieties and mineral species (Table 1) are very broad, and overtones should reproduce the general shape of those fundamentals. There is no evidence of such in Fig. 3 for SM2 grain #40 or SM12 grain #12. In particular, the CH stretch modes are much sharper than any possible overtone band, so that the latter would mainly affect the baseline, which has been subtracted off. Moreover, if the aliphatic C-H bands had significant contribution from, say, carbonate overtones, their spatial distributions (Figs. 4c, 4e, 5c, and 5e) would be more similar than observed.

CONCLUSION

Synchrotron-based microscale FTIR spectroscopy of Sutter's Mill meteorites SM2 and SM12 shows that the spatial distributions of carbonates and both aromatic and aliphatic hydrocarbons are negatively correlated. The spatial distribution of aliphatic organic matter and OH relative to the distributions of silicates in SM2 differs somewhat from that in SM12, supporting a hypothesis that the parent body of Sutter's Mill is a combination of multiple bodies. From the micro-Raman spectra, we confirm that SM12 experienced higher thermal metamorphism than did SM2, although SM2 contains a greater proportion of olivine. The CH_2/CH_3 ratio in Sutter's Mill is higher than found in bulk CM and CI chondrites, but it is similar to that of interplanetary dust particles and comets. These differences may indicate a different origin and/or parent body processing of the aliphatic organic matter in SM2 and SM12 than in other CM and CI chondrites and diffuse ISM objects.

Acknowledgments—We thank NASA Ames Research Center and the Sutter's Mill meteorite consortium for providing the meteorite samples. Mr. Yesiltas is primarily supported through Graduate Fellowship Program #1416 by the Turkish government. SRC is primarily funded by the University of Wisconsin-Madison with supplemental support from facility users

and the University of Wisconsin-Milwaukee. IRENI beamline's construction and development was supported by NSF MRI award # 0619759, and CJH is funded by NSF CHE award # 1112433. We are also grateful to associate editor Dr. S. Sandford and the reviewers for constructive comments on this manuscript.

Editorial Handling—Dr. Scott Sandford

REFERENCES

Akai J. 1992. T-T-T diagram of serpentine and saponite, and estimation of metamorphic heating degree of Antarctic carbonaceous chondrites. *Proceedings of the NIPR Symposium on Antarctic Meteorites* 5:120–135.

Alexander C. M. O'D., Cody G. D., Kebukawa Y., Bowden R., Fogel M. L., Kilcoyne A. L. D., Nittler L. R., and Herd C. D. K. 2014. Elemental, isotopic, and structural changes in Tagish Lake insoluble organic matter produced by parent body processes. *Meteoritics & Planetary Science* 49:503–525.

Beck P., Quirico E., Montes-Hernandez G., Bonal L., Bollard J., Orthous-Daunay F.-R., Howard K. T., Schmitt B., Brissaud O., Deschamps F., Wunder B., and Guillot S. 2010. Hydrous mineralogy of CM and CI chondrites from infrared spectroscopy and their relationship with low albedo asteroids. *Geochimica et Cosmochimica Acta* 74:4881–4892.

Burton A. S., Glavin D. P., Elsila J. E., Dworkin J. P., Jenniskens P., and Yin Q-Z. 2014. The amino acid composition of the Sutter's Mill CM2 carbonaceous chondrite. *Meteoritics & Planetary Science*, doi:10.1111/maps.12281.

Busemann H., Alexander C. M. O'D., and Nittler L. R. 2007. Characterization of insoluble organic matter in primitive meteorites by microRaman spectroscopy. *Meteoritics & Planetary Science* 42:1387–1416.

Cody G. D., Alexander C. M. O'D., Yabuta H., Kilcoyne A. L. D., Araki T., Ade H., Dera P., Fogel M., Militzer B., and Mysen B. O. 2008. Organic thermometry for chondritic parent bodies. *Earth and Planetary Science Letters* 272:446–455.

Flynn G. J., Keller L. P., Feser M., Wirick S., and Jacobsen C. 2003. The origin of organic matter in the solar system: Evidence from the interplanetary dust particles. *Geochimica et Cosmochimica Acta* 67:4791–4806.

Flynn G. J., Wirick S., Sandford S. A., and Nuevo M. 2013. Infrared analyses of minerals and organics in the Sutter's Mill meteorite (abstract #1595). 44th Lunar and Planetary Science Conference. CD-ROM.

Fries M., Matson R., Schaefer J., Fries J., Reddy V., Lecorre L., and Hankey M. 2014. Detection and rapid recovery of the Sutter's Mill meteorite as a model for future recoveries worldwide. *Meteoritics & Planetary Science*, doi:10.1111/maps.12249.

Haack H., Michelsen R., Stober G., Keuer D., and Singer W. 2010. The Maribo CM2 fall: Radar based orbit determination of an unusually fast fireball (abstract #5085). *Meteoritics & Planetary Science* 45:A72.

Huss G. R., Rubin A. E., and Grossman J. N. 2006. Thermal metamorphism in chondrites. In *Meteorites and the early solar system II*, edited by Lauretta D. S., Leshin L. A., and McSween H. Y. Jr. Tucson, Arizona: The University of Arizona Press. pp. 567–586.

Igisu M., Ueno Y., Shimojima M., Nakashima S., Awramik S. M., Ohta H., and Maruyama S. 2009. Micro-FTIR spectroscopic signatures of bacterial lipids in proterozoic microfossils. *Precambrian Research* 173:19–26.

Jenniskens P., Fries M. D., Yin Q.-Z., Zolensky M., Krot A. N., Sandford S. A., Sears D., Beauford R., Ebel D. S., Friedrich J. M., Nagashima K., Wimpenny J., Yamakawa A., Nishiizumi K., Hamajima Y., Caffee M. W., Welten K. C., Laubenstein M., Davis A. M., Simon S. B., Heck P. R., Young E. D., Kohl I. E., Thiemens M. H., Nunn M. H., Mikouchi T., Hagiya K., Ohsumi K., Cahill T. A., Lawton J. A., Barnes D., Steele A., Rochette P., VerosubK L., Gattacceca J., Cooper G., Glavin D. P., Burton A. S., Dworkin J. P., Elsila J. E., Pizzarello S., Ogliore R., Schmitt-Kopplin P., Harir M., Hertkorn N., Verchovsky A., Grady M., Nagao K., Okazaki R., Takechi H., Hiroi T., Smith K., Silber E. A., Brown P. G., Albers J., Klotz D., Hankey M., Matson R., Fries J. A., Walker R. J., Puchtel I., Lee C.-T. A., Erdman M. E., Eppich G. R., Roeske S., Gabelica Z., Lerche M., Nuevo M., Girten B., and Worden S. P. 2012. Radar-enabled recovery of the Sutter's Mill meteorite, a carbonaceous chondrite regolith breccia. *Science* 338:1583–1587.

Kebukawa Y., Nakashima S., Nakamura-Messenger K., and Zolensky M. E. 2009a. Submicron distribution of organic matter of carbonaceous chondrite using near-field infrared microspectroscopy. *Chemistry Letters* 38:22–23.

Kebukawa Y., Nakashima S., Nakamura-Messenger K., and Zolensky M. E. 2009b. Rapid contamination during storage of carbonaceous chondrites prepared for micro FTIR measurements. *Meteoritics & Planetary Science* 44:545–557.

Kebukawa Y., Nakashima S., Ishikawa M., Aizawa K., Inoue T., Nakamura-Messenger K., and Zolensky M. E. 2010. Spatial distribution of organic matter in the Bells CM2 chondrite using near-field infrared micro-spectroscopy. *Meteoritics & Planetary Science* 45:394–405.

Keller L. P., Bajt S., Baratta G. A., Borg J., Bradley J. P., Brownlee D. E., Brucato J. R., Burchell M. J., Busemann H., Colangeli L., D'Hendecourt L., Djouadi Z., Ferrini G., Flynn G., Franchi I. A., Fries M., Grady M. M., Gilles M. K., Graham A., Grossemy F., Kearsley A., Matrajt G., Nakamura-Messanger K., Mennella V., NittlerL R., Palumbo M. E., Rotundi A., Sandford S. A., Snead C. J., Stadermann F. J., Steele A., Tsou P., Wooden D., and Zolensky M. 2006. Infrared spectroscopy of comet 81P/Wild 2 samples returned by Stardust. *Science* 314:1728–1731.

Matrajt G., Borg J., Raynal P. I., Djouadi Z., d'Hendecourt L., Flynn G., and Deboffle D. 2004. FTIR and Raman analyses of the Tagish Lake meteorite: Relationship with the aliphatic hydrocarbons observed in the Diffuse Interstellar Medium. *Astronomy & Astrophysics* 416:983–990.

Merouane S., Djouadi Z., d'Hendecourt L. L. S., Zanda B., and Borg J. 2012. Hydrocarbon materials of likely interstellar origin from the Paris meteorite. *The Astrophysical Journal* 756:154–160.

Nakamura T. 2005. Post-hydration thermal metamorphism of carbonaceous chondrites. *Journal of Mineralogical and Petrological Sciences* 100:260–272.

Nakato A., Nakamura T., Kitajima F., and Noguchi T. 2008. Evaluation of dehydration mechanism during heating of hydrous asteroids based on mineralogical and chemical analysis of naturally and experimentally heated CM chondrites. *Earth, Planets and Space* 60:855–864.

Nasse M. J., Reininger R., Kubala T., Janowski S., and Hirschmugl C. 2007. Synchrotron infrared microspectroscopy imaging using a multi-element detector (IRMSI-MED) for diffraction-limited chemical imaging. *Nuclear Instruments and Methods in Physics Research Section A—Accelerators Spectrometers Detectors and Associated Equipment* 582:107–110.

Nasse M. J., Mattson E. C., Reininger R., Kubala T., Janowski S., El-Bayyari Z., and Hirschmugl C. J. 2011. Multi-beam synchrotron infrared chemical imaging with high spatial resolution: Beam line realization and first reports on image restoration. *Nuclear Instruments and Methods in Physics Research Section A—Accelerators Spectrometers Detectors and Associated Equipment* 649:172–176.

Nuevo M., Sandford S. A., Flynn G. J., and Wirick S. 2014. Mid-IR study of stones from the Sutter's Mill meteorite. *Meteoritics & Planetary Science*, doi:10.1111/maps.12269.

Osawa T., Kagi H., Nakamura T., and Noguchi T. 2005. Infrared spectroscopic taxonomy for carbonaceous chondrites from speciation of hydrous components. *Meteoritics & Planetary Science* 40:71–86.

Pearson V. K., Sephton M. A., Kearsley A. T., Bland P. A., Franchi I. A., and Gilmour I. 2002. Clay mineral-organic matter relationships in the early solar system. *Meteoritics & Planetary Science* 37:1829–1833.

Pearson V. K., Kearsley A. T., Sephton M. A., and Gilmour I. 2007. The labelling of meteoritic organic material using osmium tetroxide vapour impregnation. *Planetary and Space Science* 55:1310–1318.

Pizzarello S., Davidowski S. K., Holland G. P., and Williams L. B. 2013. Processing of meteoritic organic materials as a possible analog of early molecular evolution in planetary environments. *Proceedings of the National Academy of Sciences* 110:15,614–15,619.

Salisbury J. W., Walter L. S., Vergo N., and D'Aria D. M. 1991. *Infrared (2.1-25 μm) spectra of minerals*. Baltimore, Maryland: John Hopkins University Press. 267 pp.

Sandford S. A. 1984. Infrared transmission spectra from 2.5 to 25 microns of various meteorite classes. *Icarus* 60:115–126.

Sandford S., Allamandola L., Tielens A., Sellgren K., Tapia M., and Pendleton Y. 1991. The interstellar CH stretching band near 3.4 microns—Constraints on the composition of organic material in the diffuse interstellar medium. *The Astrophysical Journal* 371:607–620.

Sandford S. A., Aléon J., Alexander C. M. O'D., Araki T., Bajt S. A., Baratta G. A., Borg J., Bradley J. P., Brownlee D. E., and Brucato J. R. 2006. Organics captured from comet 81P/Wild 2 by the Stardust spacecraft. *Science* 314:1720–1724.

Sandford S., Nuevo M., Flynn G., and Wirick S. 2013. Mid-infrared study of samples from several stones from the Sutter's Mill meteorite (abstract #1663). 44th Lunar and Planetary Science Conference. CD-ROM.

Suzuki A., Yamanoi Y., Nakamura T., and Nakashima S. 2010. Micro-spectroscopic characterization of organic and hydrous components in weathered Antarctic micrometeorites. *Earth, Planets and Space* 62:33–46.

Takir D., Emery J. P., McSween H. Y., Hibbits C. A., Clark R. N., Pearson N., and Wang A. 2013. Nature and degree of aqueous alteration in CM and CI carbonaceous chondrites. *Meteoritics & Planetary Science* 48:1618–1637.

Yesiltas M., Hirschmugl C., and Peale R. 2013. In situ investigation of meteoritic organic-mineral relationships by high spatial resolution infrared spectroscopy (abstract #5068). *Meteoritics & Planetary Science* 48.

Zolensky M., Mikouchi T., Fries M., Bodnar R., Jenniskens P., Yin Q-Z., Hagiya K., Ohsumi K., Komatsu M., Colbert M., Nakamura T., Matsuoka M., Sasaki S., Tsuchiyama A., Gounelle M., Le L., Martinez J., and Ross K. 2014. Mineralogy and petrography of C asteroid regolith: The Sutter's Mill. *Meteoritics & Planetary Science*, doi:10.1111/maps.12386.